LA-UR- 09-00011

*Approved for public release;*
*distribution is unlimited.*

| | |
|---|---|
| *Title:* | MODELING CRYSTAL PLASTICITY MICROSTRUCTURES USING LAMINATES WITH HARDENING |
| *Author(s):* | Benjamin Hanseng, 189612<br>Curt Bronkhorst, 189782<br>Michael Ortiz, Cal. Inst. of Tech |
| *Intended for:* | International Symposium on Plasticity<br>St. Thomas, U.S. Virgin Islands<br>1/3-9/09 |

Los Alamos
NATIONAL LABORATORY
EST. 1943



Form 836 (7/06)

# Abstract

A single crystal plasticity theory for insertion into finite element simulation is formulated using sequential laminates to model subgrain dislocation structures. It is known that local models do not adequately account for latent hardening, as latent hardening is not only a material property, but a non-local property (e.g. grain size and shape). The addition of the non-local energy from the formation of subgrain structure dislocation walls and the boundary layer misfits provide both latent and self hardening of crystal slip. Latent hardening occurs as the formation of new dislocation walls limit motion of new mobile dislocations thus hardening future slip systems. Self hardening is accomplished by evolution of the subgrain structure length scale. No multiple slip hardening terms are included.

The substructure length scale is computed by minimizing the non-local energy. The minimization of the non-local energy is a competition between the dislocation wall and boundary layer energy. The non-local terms are also directly minimized within the subgrain model as they impact deformation response. The geometrical relationship between the dislocation walls and slip planes affecting dislocation mean free path is accounted for giving a first-order approximation to shape effects. A coplanar slip model is developed due to requirements when modeling the subgrain structure. This subgrain structure plasticity model is noteworthy as all material parameters are experimentally determined rather than

fit. The model also has an inherit path dependency due to the formation of the subgrain structures. Validation is accomplished by comparison to single crystal tension experiments.

# Modeling Crystal Plasticity Microstructures using Laminates with Hardening

Benjamin L. Hansen[1,2], Curt Bronkhorst[1], Michael Ortiz[2]

1- Los Alamos National Laboratory
2- California Institute of Technology

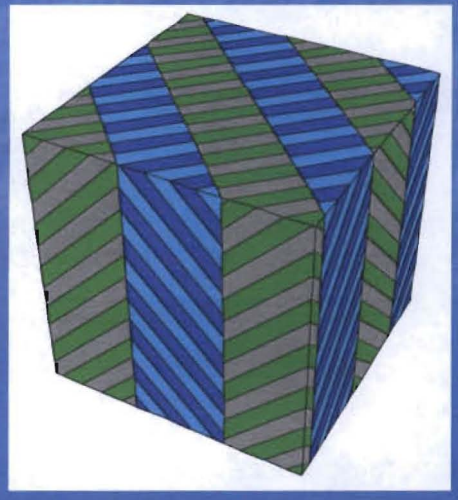

# Motivation

- Crystal Plasticity in FEM
- Latent hardening in crystal plasticity is a non-local property, dependent on grain size and shape. Non-local properties not captured in local models.
- Local models with microstructure exhibit no latent hardening.
- Subgrain dislocation structures resemble laminates.
- Laminate structures can be mathematically simulated.
- Hardening can be captured by introduction of non-local subgrain structures.

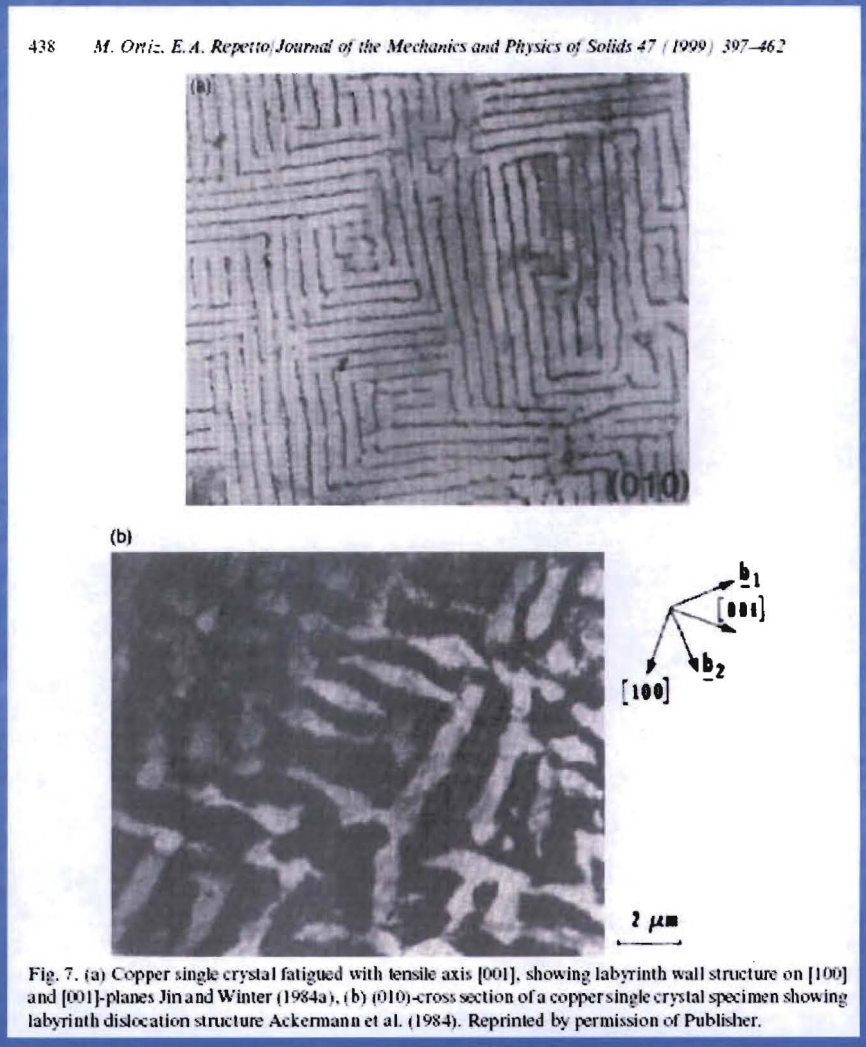


Fig. 7. (a) Copper single crystal fatigued with tensile axis [001], showing labyrinth wall structure on [100] and [001]-planes Jin and Winter (1984a), (b) (010)-cross section of a copper single crystal specimen showing labyrinth dislocation structure Ackermann et al. (1984). Reprinted by permission of Publisher.

# Single Crystal

- Elasticity Model
- Plasticity Model
- Subgrain Structures
  - Non-local Energy
- Validation
  - Single Crystal Tensile Experiments
  - Crystal Grain Shape and Size Effects

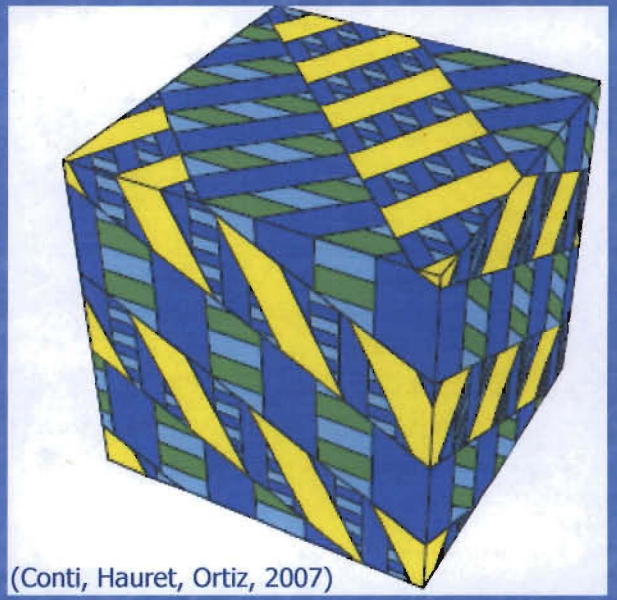

(Conti, Hauret, Ortiz, 2007)

# Laminate Microstructures

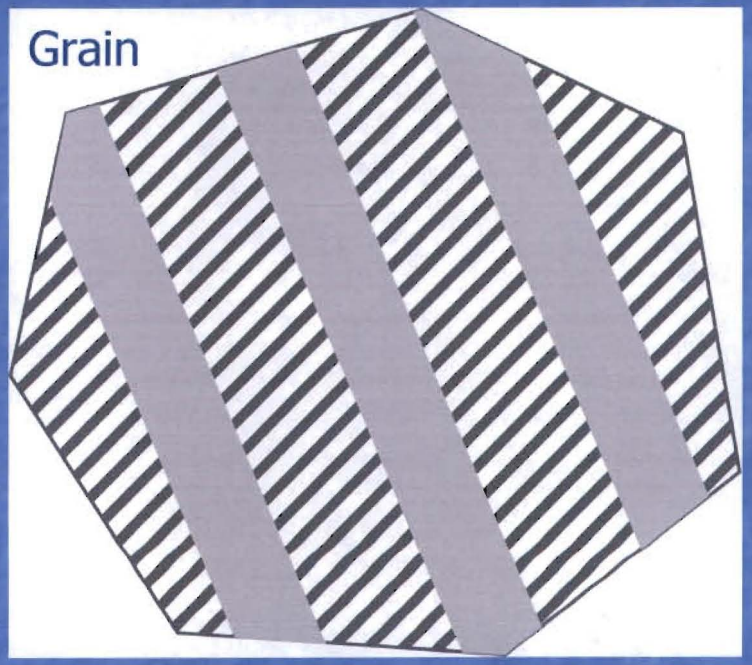


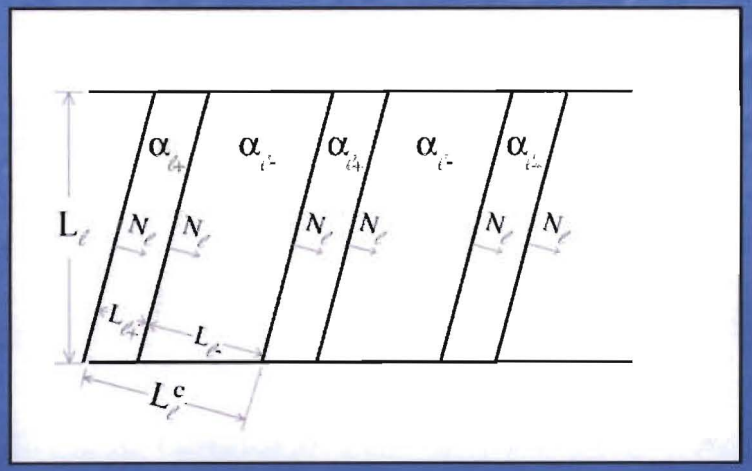


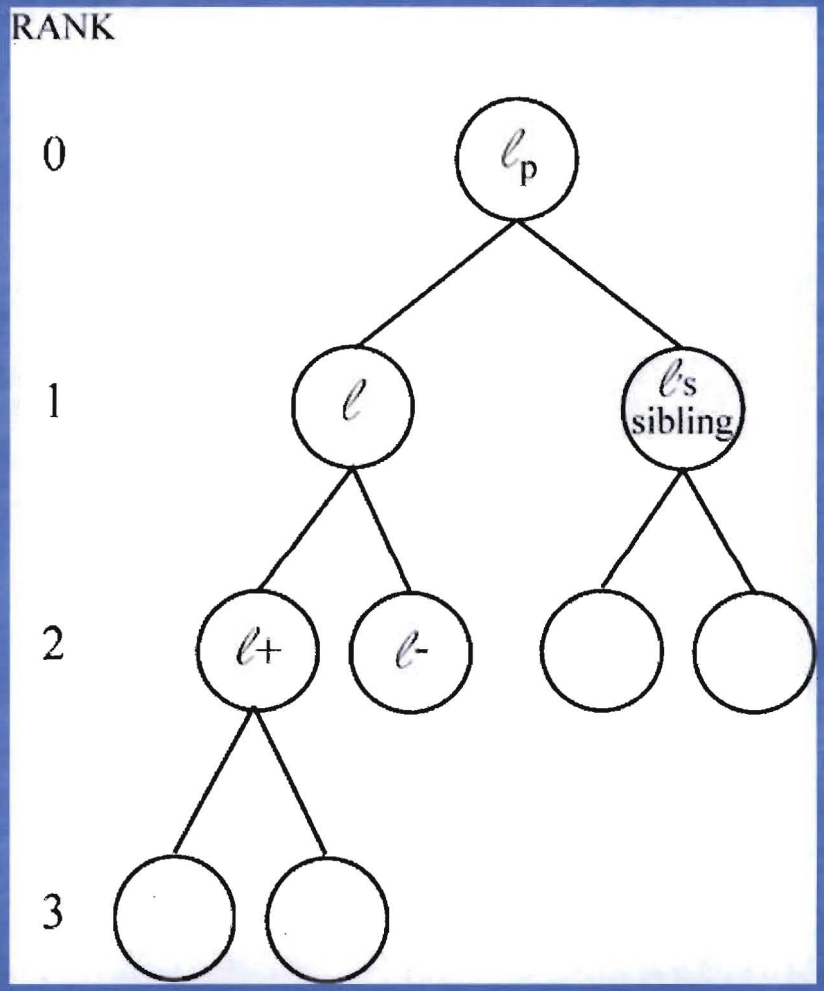

# Laminate Microstructures

Characterized by:

- a = polarization
- N = wall normal
- $\lambda$ = volume fraction
- $L^c$ = length scale

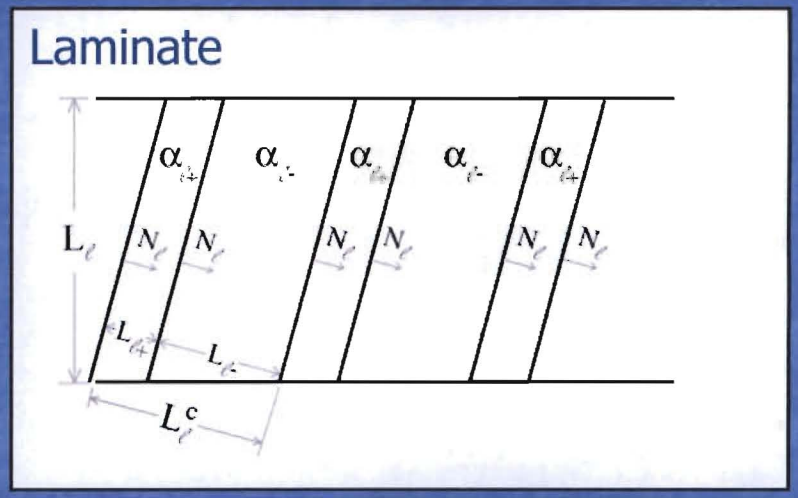


$$ {}_n\mathbf{F}_{l+} - {}_n\mathbf{F}_{l-} = {}_n\mathbf{a}_l \otimes \mathbf{N}_l $$

$$ {}_n\mathbf{P}_l = (\lambda_{l-})({}_n\mathbf{P}_{l+}) + (\lambda_{l+})({}_n\mathbf{P}_{l+}) $$

$$ {}_n\mathcal{C}_l^{laminate} = (\lambda_{l+})({}_n\mathcal{C}_{l+}^{s.s.}) + (\lambda_{l-})({}_n\mathcal{C}_{l-}^{s.s.}) $$

$$ {}_nL_l^c \equiv {}_nL_{l+} + {}_nL_{l-} \qquad {}_nL_l^c \leq {}_nL_{l_p} $$

$$ {}_nW_l[{}_n\mathbf{F}_l] \equiv \min_{\alpha_{l\pm}, a_l, N_l, \lambda_{l\pm}, L_l^c} \left( \lambda_{l-}\ {}_nW_{l-} + \lambda_{l+}\ {}_nW_{l+} + \left({}_{(n-1)}\tau_l\right)\left({}_{(n-1)}\gamma_l\right) + 2\Upsilon \frac{{}_nL_l^c}{{}_{n-1}L_l}\, {}_nW_l^{BL} \right) $$

$$ {}_nW_l^{NL} = {}_nW_l^{DW} + 2\Upsilon \frac{{}_nL_l^c}{{}_{n-1}L_l}\, {}_nW_l^{BL} $$

$$ {}_nL_l^c = \sqrt{\frac{T\ {}_{n-1}L_l}{2\Upsilon b\ {}_nW_l^{BL}} \left( \frac{{}_n\gamma_{l-}}{\zeta_{l-}\lambda_{l-}} \sqrt{1 - (\mathbf{m}_{l-} \cdot \mathbf{n}_l)^2} + \frac{{}_n\gamma_{l+}}{\zeta_{l+}\lambda_{l+}} \sqrt{1 - (\mathbf{m}_{l+} \cdot \mathbf{n}_l)^2} \right)} $$

# Elasticity Model

- Separation of Elastic and Plastic Deformation
  - Multiplicative Decomposition of the deformation gradient

$$\mathbf{F} = \mathbf{F}^e \mathbf{F}^p$$

  - Additive separation of Elastic and Plastic Energy

$$\phi = W^e[\mathbf{F}^e] + W^p[\mathbf{F}^p, \gamma]$$

- Elastic Single Crystal Model
  - Constitutive

$$\mathbf{E}^e = \frac{1}{2}((\mathbf{F}^e)^T \mathbf{F}^e - \mathbf{I})$$

$$\mathbf{K}^e = \mathcal{C}^{mat} \cdot \mathbf{E}^e$$

$$\mathbf{P}^e = \mathbf{F}^e \mathbf{K}^e$$

  - Energy

$$W^e = \frac{1}{2} \mathbf{K}^e \cdot \mathbf{E}^e$$

  - Material Tangent

$$\mathcal{C}^e_{iJkL} = \frac{\partial \mathbf{P}^e}{\partial \mathbf{F}^e} = \delta_{ik} K^e_{JL} + 2 F^e_{iM} F^e_{kN} C^{mat}_{MJNL}$$

# Plasticity Model

- Due to latent hardening + formation of microstructure, single slip is energetically favorable. (Conti and Ortiz, 2005; Ortiz and Repetto, 1999)
- Irreversibility and Crit. Resolved Shear Stress give conditions for slip

$$\tau_\alpha - g_\alpha \leq 0, \quad \dot{\gamma}_\alpha \geq 0, \quad (\tau_\alpha - g_\alpha)\dot{\gamma}_\alpha = 0$$

- Flow Rule

$${}_{n+1}\mathbf{F}^p = (\mathbf{I} + \sum_{\alpha=1}^{N} \Delta\gamma_\alpha \mathbf{s}_\alpha \otimes \mathbf{m}_\alpha)_n\mathbf{F}^p$$

- Energy

$${}_nW^p = \sum_{\alpha=1}^{N} ({}_n\tau_\alpha)({}_n\gamma_\alpha)$$

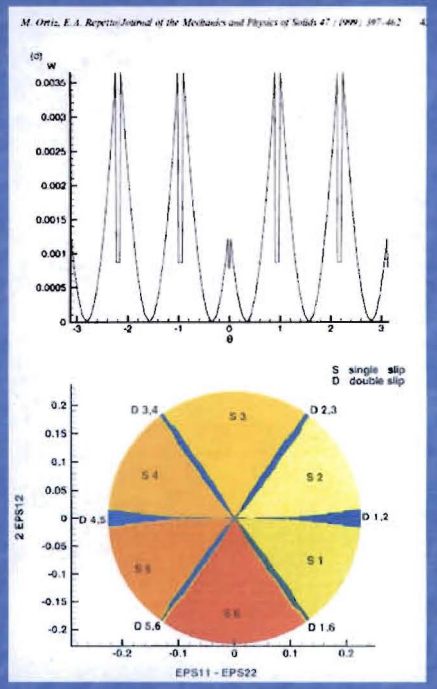


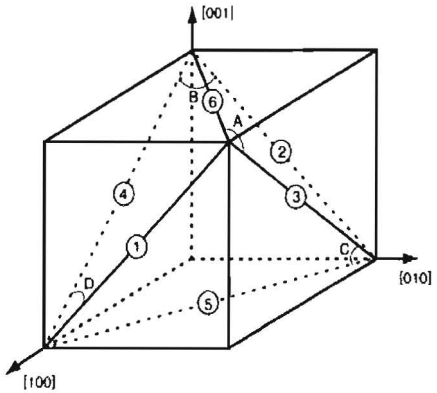


Table 2.1: FCC slip systems

| System | A2 | A3 | A6 | B2 | B4 | B5 | C1 | C3 | C5 | D1 | D4 | D6 |
|---|---|---|---|---|---|---|---|---|---|---|---|---|
| $s*\sqrt{2}$ | $\pm[0\bar{1}1]$ | $\pm[101]$ | $\pm[110]$ | $\pm[0\bar{1}1]$ | $\pm[\bar{1}01]$ | $\pm[\bar{1}10]$ | $\pm[011]$ | $\pm[101]$ | $\pm[\bar{1}10]$ | $\pm[011]$ | $\pm[\bar{1}01]$ | $\pm[110]$ |
| $m*\sqrt{3}$ | $(\bar{1}11)$ | $(\bar{1}11)$ | $(\bar{1}11)$ | $(111)$ | $(111)$ | $(111)$ | $(\bar{1}\bar{1}1)$ | $(\bar{1}\bar{1}1)$ | $(\bar{1}\bar{1}1)$ | $(1\bar{1}1)$ | $(\bar{1}\bar{1}1)$ | $(\bar{1}\bar{1}1)$ |

# Coplanar Slip

- Although coplanar slip forms laminate microstructures, these subgrain structures do not contain dislocation walls. Also formed at very fine scale.
- Leads to forming a theory where each laminate contains all coplanar slip.
- Coplanar Slip Theory:
  - Effective slip direction:

$$ {}_n\hat{\mathbf{s}} \equiv \sum_{\alpha \in coplanar} \frac{\dot{\gamma}_\alpha}{\dot{\gamma}_T} s_\alpha $$

$$ \dot{\gamma}_T \equiv \sum_{\alpha \in coplanar} \dot{\gamma}_\alpha $$

Note, it is not normalized.

$$ \Delta_n W^p = {}_n\tau^c \gamma_T $$

$$ \begin{aligned} {}_n\mathbf{F}_l^p &= (\mathbf{I} + {}_n\gamma_T \hat{\mathbf{s}}_\alpha \otimes \mathbf{m})({}_{n-1}\mathbf{F}_l^p) \\ &= (\mathbf{I} + (\sum_\alpha {}_n\gamma_\alpha \mathbf{s}_\alpha) \otimes \mathbf{m})({}_{n-1}\mathbf{F}_l^p) \\ &= (\mathbf{I} + (\sum_\alpha {}_n\gamma_\alpha \mathbf{s}_\alpha \otimes \mathbf{m}))({}_{n-1}\mathbf{F}_l^p) \end{aligned} $$

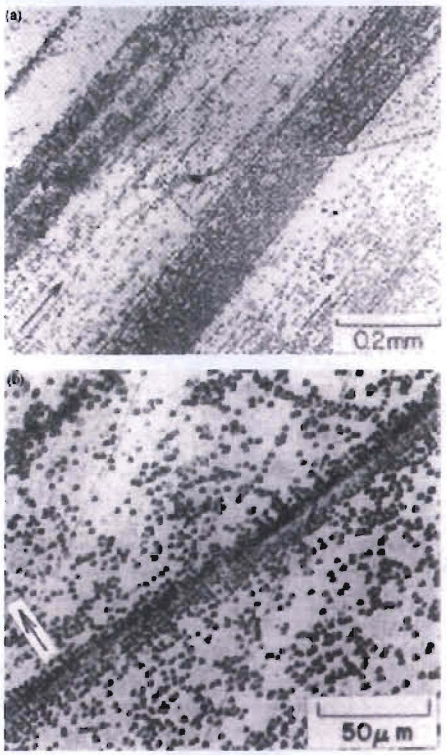


Fig. 14. Cu-1at.%Ge alloy crystal oriented near [321] and deformed monotonically to 30% strain. Higashida et al. (1986). (a) Coplanar slip zones revealed by etch pits on the conjugate plane. (b) etch pit configuration due to secondary dislocations in the vicinity of kink bands. Reprinted by permission of Publisher.

# Coplanar Slip

- Solution for Coplanar Slip Effective Direction
  - Desire condition: $_n\tau_{alpha} = _n tau_c \; for \; all \; \alpha \in \; coplanar$
  - Initial guess for effective slip direction

$$F^e \approx \mathbf{I}$$

$$\begin{aligned} \omega_a &= \tau_\alpha - \tau_\alpha^c \\ d &= \mathbf{s}_1 \cdot \mathbf{s}_2 \end{aligned}$$

$$\hat{\mathbf{s}}_0 = \frac{(\omega_1 - \omega_2 d)}{(\omega_1 + \omega_2)(1-d)}\mathbf{s}_1 + \frac{(\omega_2 - \omega_1 d)}{(\omega_1 + \omega_2)(1-d)}\mathbf{s}_2$$

  - Further driven to match condition by iteration

$$\frac{\partial_n \tau_\alpha - {}_n\tau_\alpha^c}{\partial \gamma_\beta} = -({}_n\mathbf{F}^e \mathbf{s}_\alpha \otimes \mathbf{m}_\alpha) \cdot \mathcal{C}^e \cdot (n+1\mathbf{F}^e \mathbf{s}_\beta \otimes \mathbf{m}_\beta)$$

  - Solution scheme, single or coplanar slip

1. Compute all $\tau_\alpha - \tau^c$
2. Activate maximum slip system from step 1 as single slip
3. Re-compute all $\tau_\alpha - \tau^c$

   if all $\tau_\alpha - \tau^c \leq 0, exit$

   else, return max $\alpha$ slip system to original slip strain and activate two highest $\tau_\alpha - \tau^c$. Exit.

# Mean Free Path Shortening

- When dislocation walls form the mean free path of dislocations is shortened.

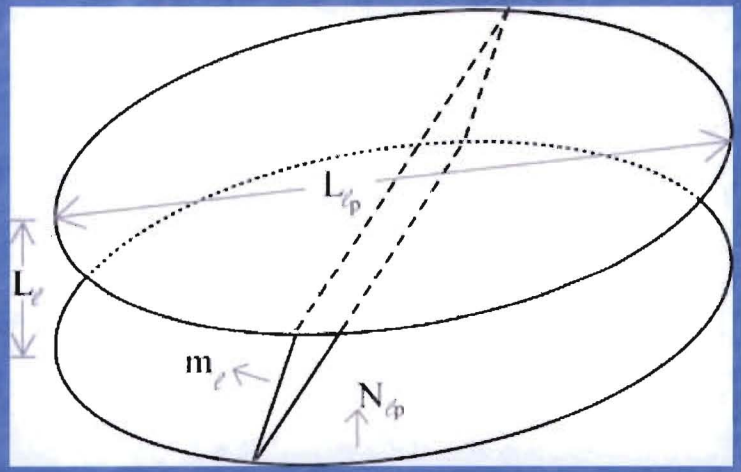


- The actual length depends on the angle between the slip plane and the dislocation wall.

$$A = \frac{L_l}{\sqrt{1-(\mathbf{m}_l \cdot \mathbf{N}_{l_p})^2}}$$
$$B = L_{l_p}$$

# Mean Free Path

$$h_l \equiv \frac{\sum paths}{\#paths}$$

Assuming the direction of motion of the dislocations is uniformly distributed and dislocations are available everywhere

$$\#paths = \int_{\Omega} \int_{\alpha=0}^{\alpha=2\pi} d\alpha \; d\bar{x} = 2\pi AB$$

$$\sum paths = \int_{\Omega} \int_{\alpha=0}^{\alpha=2\pi} p[\alpha, \bar{x}] d\alpha \; d\bar{x}$$

Assuming separation of length scales, several small angle approximations can be made yielding:

$$h_l = \zeta_l A_l = \frac{\zeta_l L_l}{\sqrt{1 - (\mathbf{m}_l \cdot \mathbf{N}_{l_p})^2}}$$

# Eliminating parent length

Table 3.1: L/A ratios for generic slip system A6

| System | $\mathbf{n} * \sqrt{3}$ | $\frac{L_{A6}}{A_{A6}}$ |
|---|---|---|
| A2 | $(\bar{1}11)$ | 0 |
| A3 | $(\bar{1}11)$ | 0 |
| A6 | $(\bar{1}11)$ | 0 |
| B2 | $(11\bar{3})$ | $2\sqrt{\frac{2}{11}}$ |
| | $(211)$ | 1 |
| B4 | $(011)$ | $\frac{1}{\sqrt{3}}$ |
| | $(11\bar{1})$ | $\frac{2}{3}\sqrt{2}$ |
| B5 | $(100)$ | $\sqrt{\frac{2}{3}}$ |
| | $(00\bar{1})$ | $\sqrt{\frac{2}{3}}$ |
| C1 | $(10\bar{1})$ | $\frac{1}{\sqrt{3}}$ |
| | $(111)$ | $\frac{2}{3}\sqrt{2}$ |
| C3 | $(12\bar{1})$ | 1 |
| | $(113)$ | $2\sqrt{\frac{2}{11}}$ |
| C5 | $(001)$ | $\sqrt{\frac{2}{3}}$ |
| | $(0\bar{1}0)$ | $\sqrt{\frac{2}{3}}$ |
| D1 | $(\bar{1}12)$ | $\frac{1}{3}$ |
| | $(311)$ | $4\sqrt{\frac{2}{33}}$ |
| D4 | $(13\bar{1})$ | $4\sqrt{\frac{2}{33}}$ |
| | $(13\bar{1})$ | $\frac{1}{3}$ |
| D6 | $\in$ plane containing $m_{D6}$ and $m_{A6}$ | $\in (0,1)$ |

(Ortiz and Repetto, 1999)

$$h_l = \zeta_l A_l = \frac{\zeta_l L_l}{\sqrt{1 - (\mathbf{m}_l \cdot \mathbf{N}_{l_p})^2}}$$

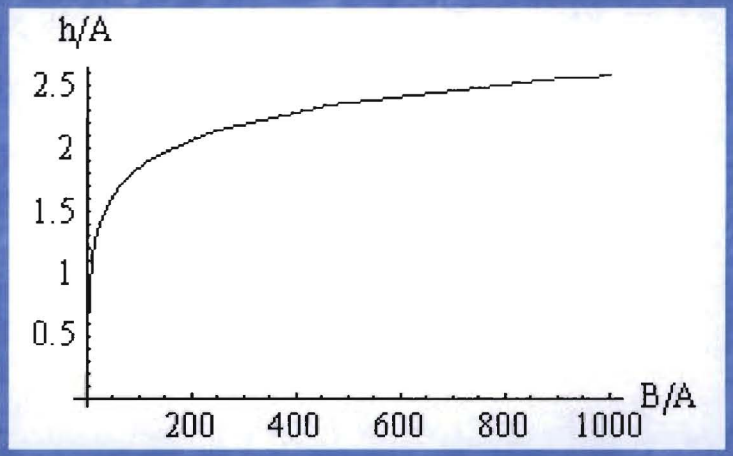


$$\zeta_l = 2$$

# Dislocation Wall Energy

- As was derived by Aubrey and Ortiz using Orowan's relation, the effect of decreasing the mean free path increases the critically resolved shear stress of the material:

$$ {}_n\tau_l^c = \tau_0^c + \frac{T}{b\ {}_n h_l} $$

- Giving a final dislocation wall energy:

$$ {}_nW_l^{DW} = \frac{T}{b}\left(\frac{{}_n\gamma_{l-}}{\lambda_{l-}\ {}_n h_{l-}} + \frac{{}_n\gamma_{l+}}{\lambda_{l+}\ {}_n h_{l+}}\right) $$

- An estimate shows this should not always be treated as a perturbation

$$ W_l^p = \tau_l^c \gamma_l $$

$$ W_l^{DW} = \frac{T\gamma_l}{bh_l} $$

$$ \Rightarrow \quad \frac{W_l^p}{W_l^{DW}} = \frac{bh_l\tau_l^c}{T} \quad \Rightarrow \quad \frac{W_l^p}{W_l^{BL}} \approx h_l * 10^6\ 1/\mathrm{m} $$

# Boundary Layer Energy

- An average of deformation in the boundary layer

$$ {}_n\mathbf{F}^{BL\pm} = \frac{1}{2}({}_n\mathbf{F}_{l\pm} + {}_n\mathbf{F}_l) $$

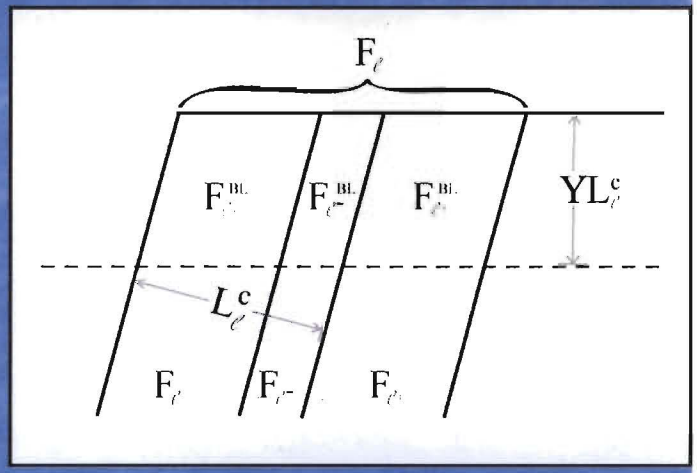


- Removing the plastic deformation that has already occurred in the parent material and assuming elastic deformation within the boundary layer yields the boundary layer energy

$$ {}_nW_l^{BL} = \lambda_{l+}(W^e[(F_{l+}^{BL})({}_n\mathbf{F}_l)^{-1}] - W[{}_nF_{l+}]) + \lambda_{l-}(W^e[(F_{l-}^{BL})({}_n\mathbf{F}_l)^{-1}] - W[{}_nF_{l-}]) $$

- Scaled by the volume of the boundary layer for the total non-local energy:

$$ W_l^{NL} = W_l^{DW} + 2\Upsilon\frac{L_l^2}{L_l}W_l^{BL} $$

# Laminate Microstructures: Non-local Energy

- The non-local energy is the combination of the energy gained from the dislocation walls and the mismatch at the boundary.

$$ {}_nW_l^{NL} = {}_nW_l^{DW} + 2\Upsilon \frac{{}_nL_l^c}{{}_{n-1}L_l} {}_nW_l^{BL} $$

- The laminate thickness is determined by the minimization of the non-local energy.

$$ {}_nL_l^c = \sqrt{\frac{T\ {}_{n-1}L_l}{2\Upsilon b\ {}_nW_l^{BL}} \left( \frac{{}^n\gamma_{l-}}{\lambda_{l-}} \sqrt{1-(\mathbf{m}_{l-}\cdot\mathbf{n}_l)^2} + \frac{{}^n\gamma_{l+}}{\lambda_{l+}} \sqrt{1-(\mathbf{m}_{l+}\cdot\mathbf{n}_l)^2} \right)} $$

$$ {}_nL_l^c = \begin{cases} \textit{equation 3.24} & \textit{,if (equation 3.24)} < {}_{n-1}L_l \\ {}_{n-1}L_l & \textit{,otherwise} \end{cases} $$

# Laminate Length Evolution

- To obtain correct time evolution of hardening it is essential to update the length of the entire microstructure:

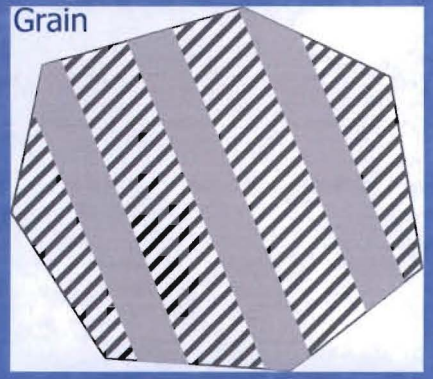


$$\min_{L_l^c,\ l=1,\ldots,Z} \sum_{l'=1}^{Z} W_{l'}^{NL}$$

$$L_l^c = \sqrt{\left(\frac{L_{l+}^c W_{l+}^{BL}}{\lambda_{l+}} + \frac{L_{l-}^c W_{l-}^{BL}}{\lambda_{l-}} + \frac{\delta_l}{2\Upsilon}\right)\frac{\lambda_l}{W_l^{BL}} L_{l_p}^c}$$

$$\delta_l \equiv \frac{T}{b\zeta}\left(\frac{\gamma_{l+}}{\lambda_{l+}}\sqrt{1-(m_{l-}\cdot N_l)^2} + \frac{\gamma_{l-}}{\lambda_{l-}} + \sqrt{1-(m_{l-}\cdot N_l)^2}\right)$$

*Note both traditional mechanisms of hardening are reproduced by the laminate size evolution: self hardening and multislip hardening.

# Boundary Conditions

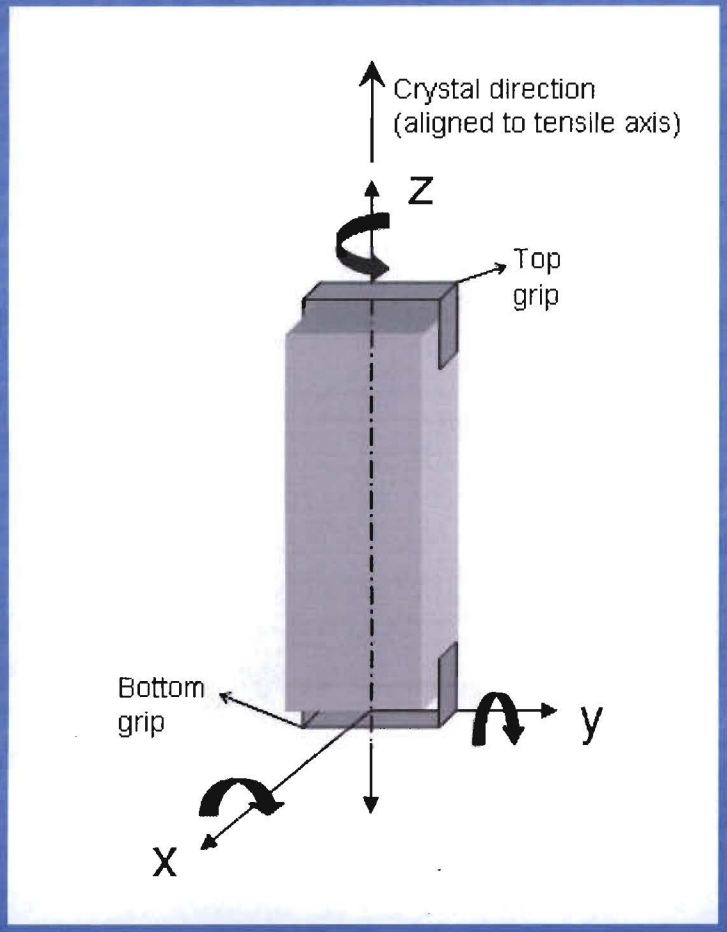


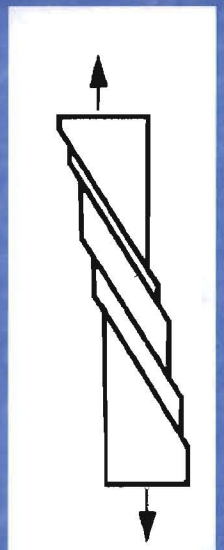

$$F = \begin{pmatrix} ? & 0 & 0 \\ 0 & ? & 0 \\ 0 & 0 & f \end{pmatrix}$$

$$P = \begin{pmatrix} 0 & ? & ? \\ ? & 0 & ? \\ ? & ? & ? \end{pmatrix}$$

Table 4.1: Copper Material Constants

| **Constant** | **Value** | **Ref.** |
|---|---|---|
| Elastic Const. ($C_{11}$) | 168.4 GPa | [GH71] |
| Elastic Const. ($C_{12}$) | 121.4 GPa | [GH71] |
| Elastic Const. ($C_{44}$) | 75.4 GPa | [GH71] |
| Crit. Shear Stress ($\tau^c$) | 1.0 MPa | [Bar52] |
| Burgers Vector ($b$) | $2.56 * 10^{-}10$ m | [KAA75] |
| Line Tension ($T$) | $18.3 * 10^{-}10$ N | [KAA75] |

# Stress Discontinuity

- There is a discontinuity in the stress when new laminates form.
- This is overcome by fixing the microstructure during the traction boundary satisfying iteration.

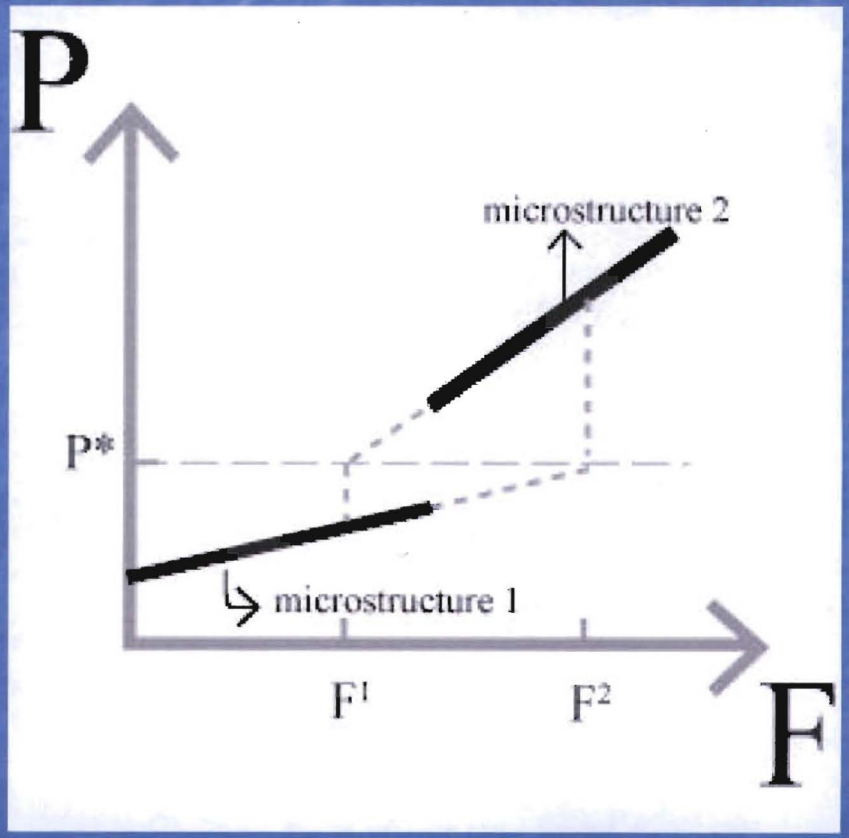

# Results – Orientation Dependence

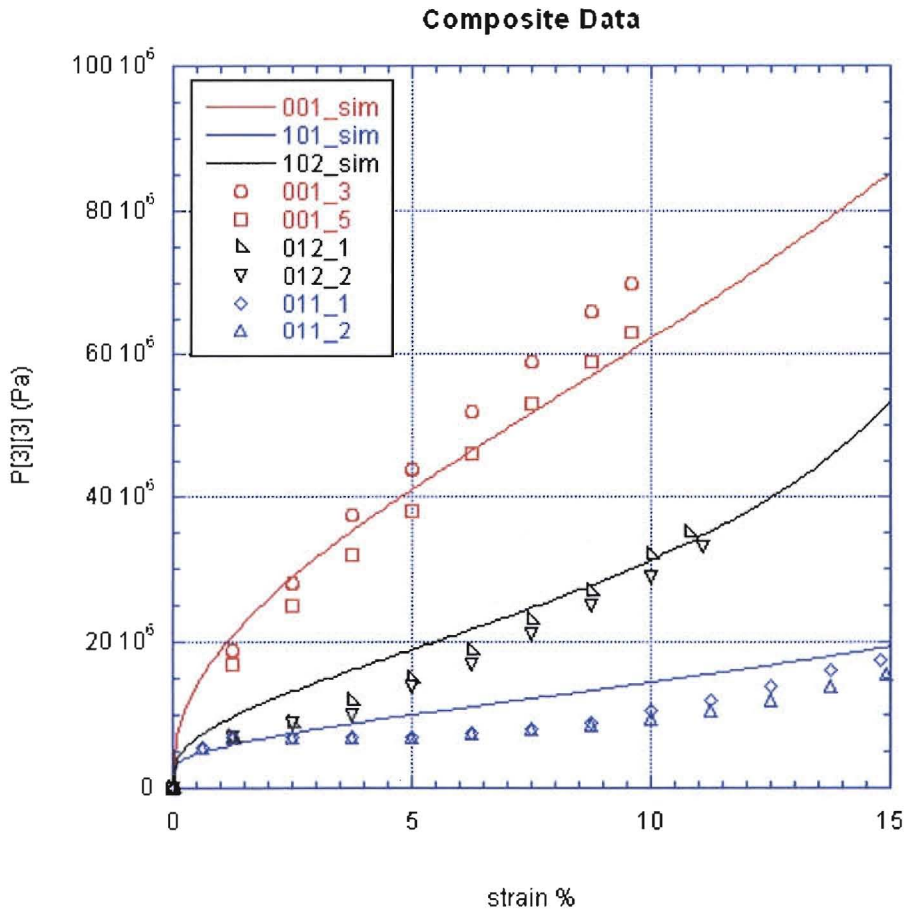


Experimental data from Franciosi, 1985.

Uncertainty in initial sample size.

# 101 Structure

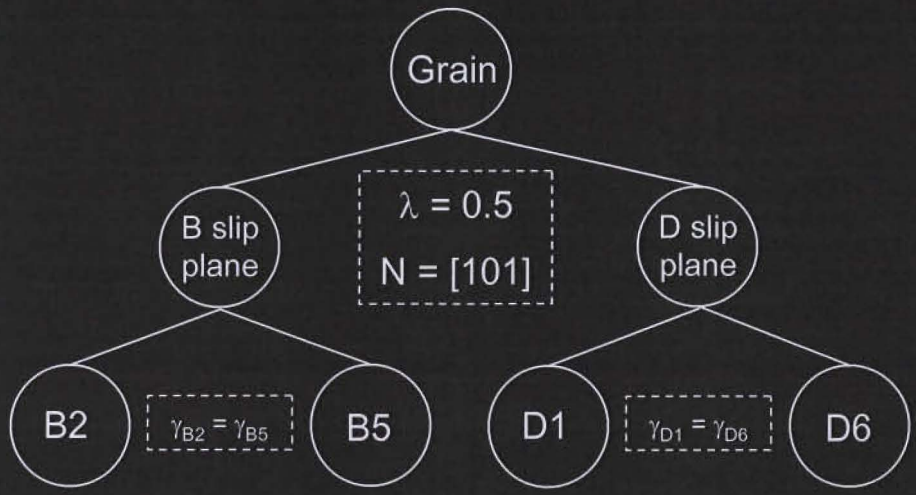


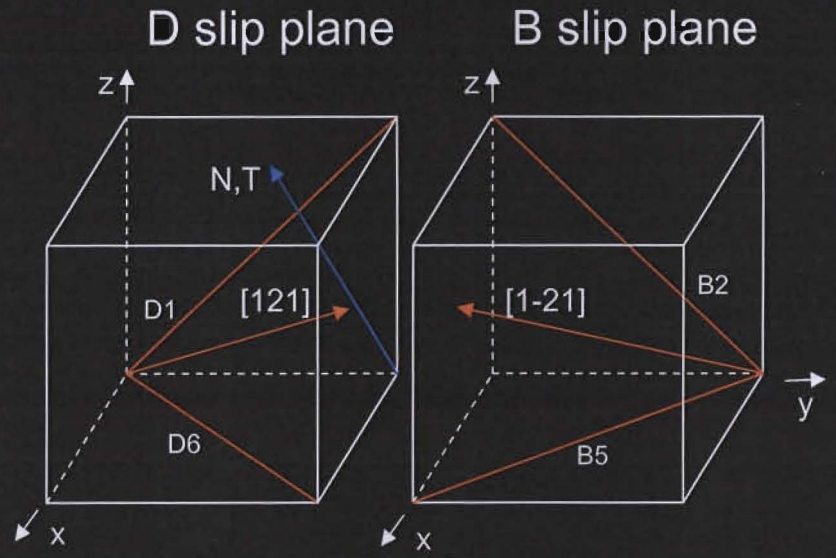


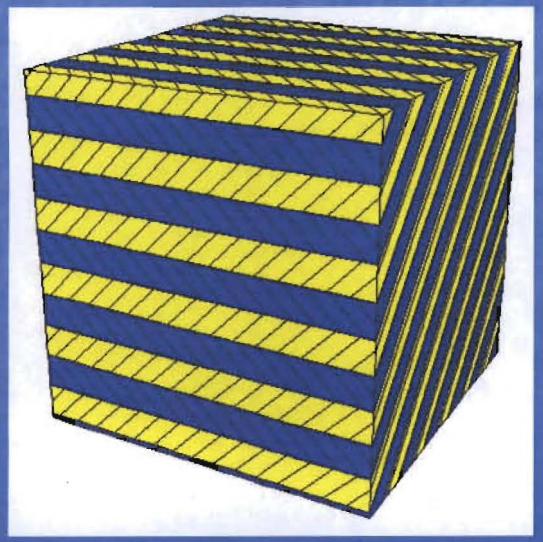

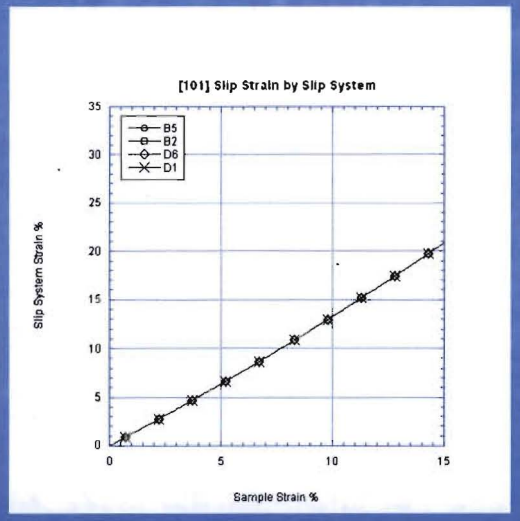


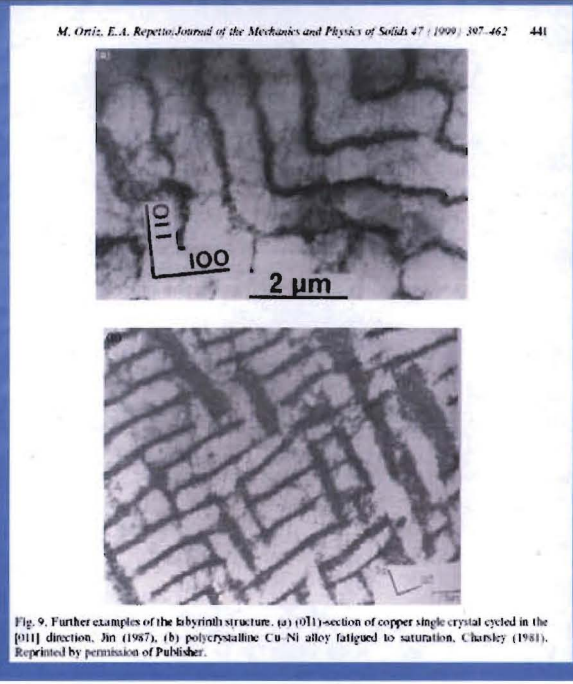


Fig. 9. Further examples of the labyrinth structure. (a) (011)-section of copper single crystal cycled in the [011] direction, Jin (1987), (b) polycrystalline Cu–Ni alloy fatigued to saturation, Charsley (1981). Reprinted by permission of Publisher.

# 102 Structure

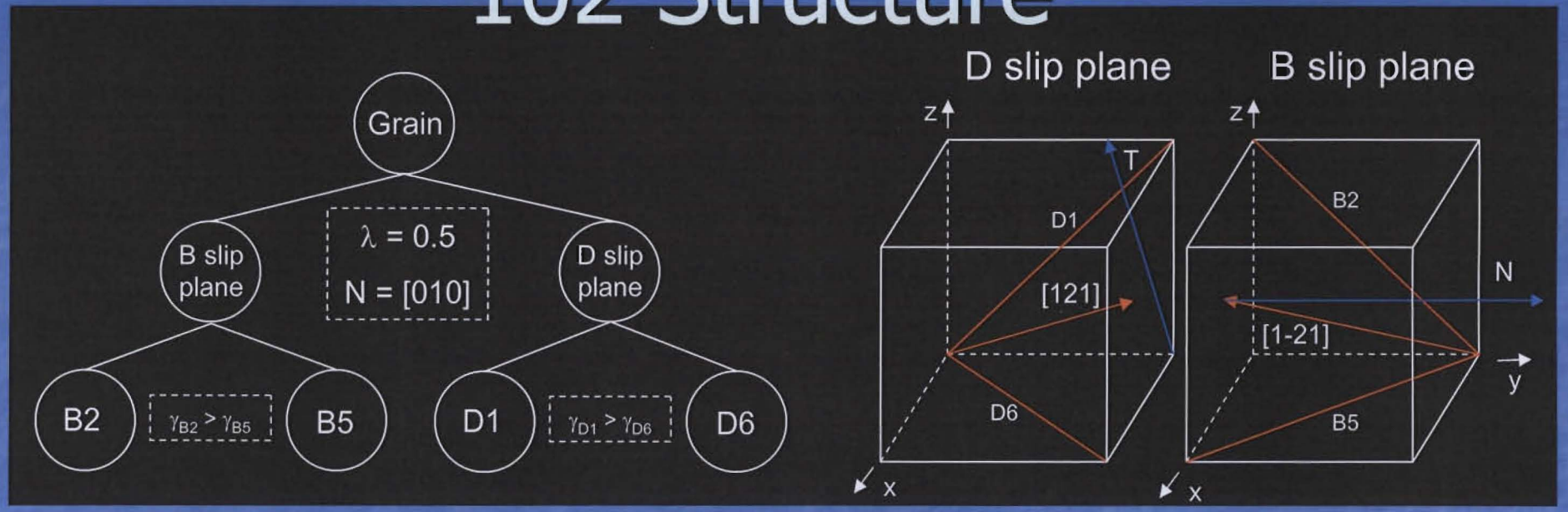


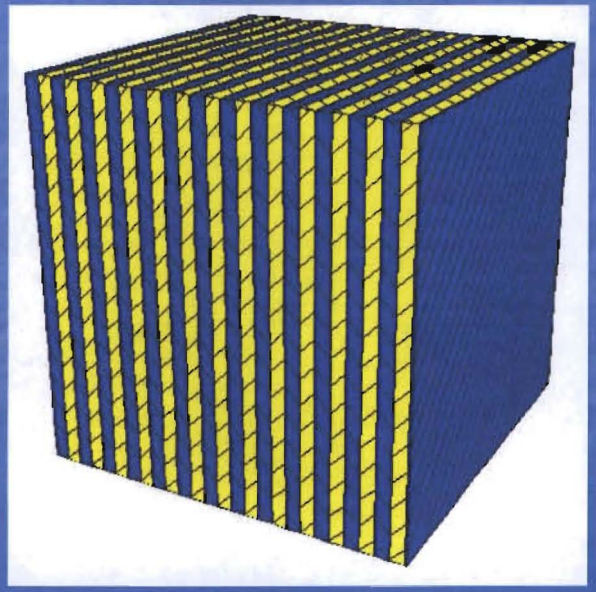

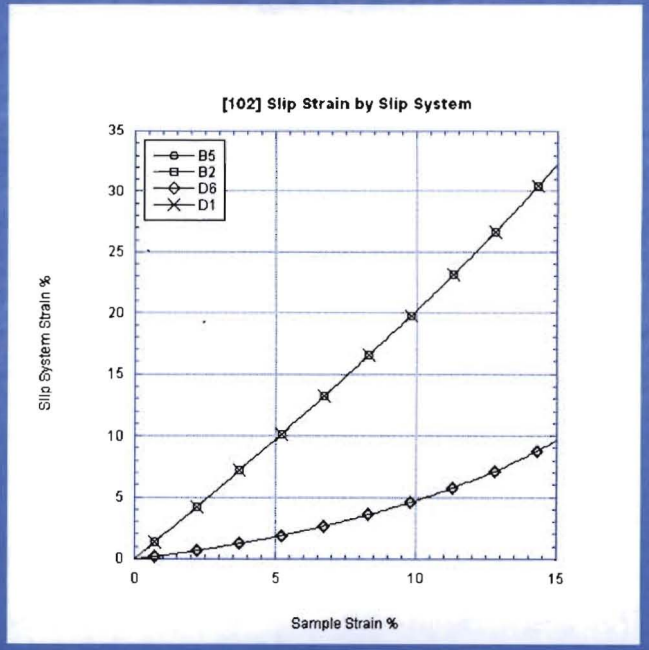

# 101 Experimental Structures



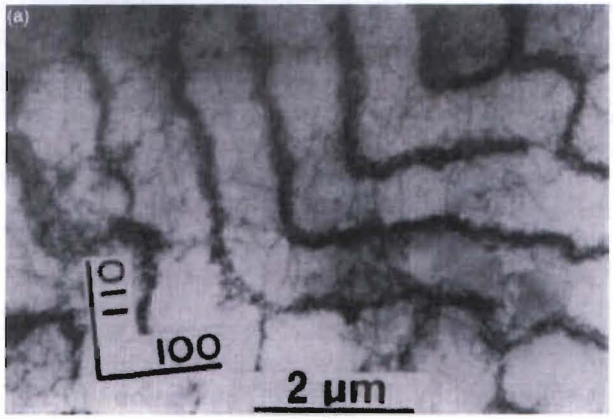


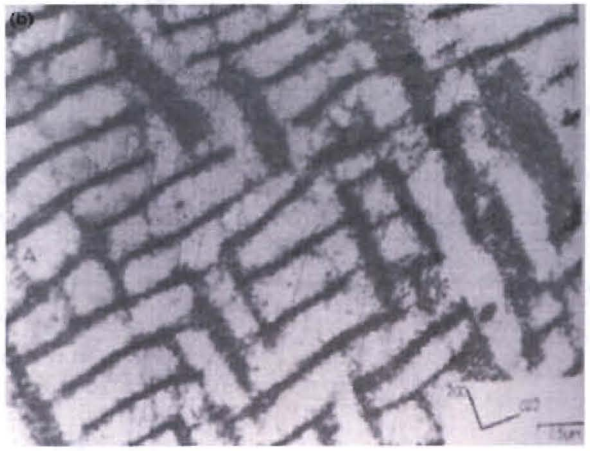


Fig. 9. Further examples of the labyrinth structure. (a) $(0\bar{1}1)$-section of copper single crystal cycled in the [011] direction, Jin (1987), (b) polycrystalline Cu–Ni alloy fatigued to saturation, Charsley (1981). Reprinted by permission of Publisher.



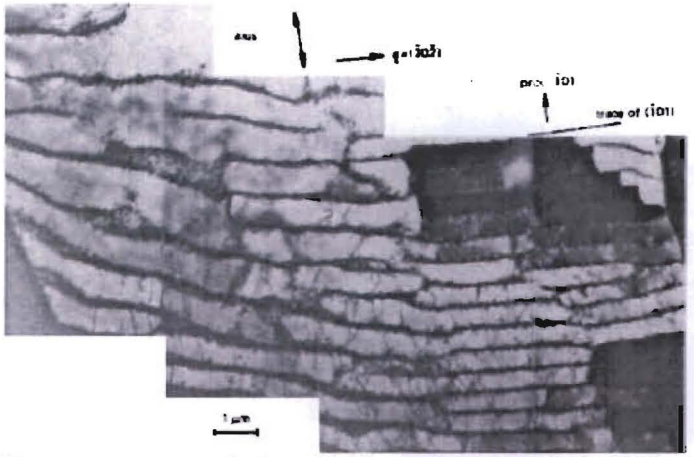


Fig. 10. (101) wall structure in fatigued polycrystalline copper, Wang and Mugharbi (1984). Reprinted by permission of Publisher.

# 001 Crystal Sub-grain Structure

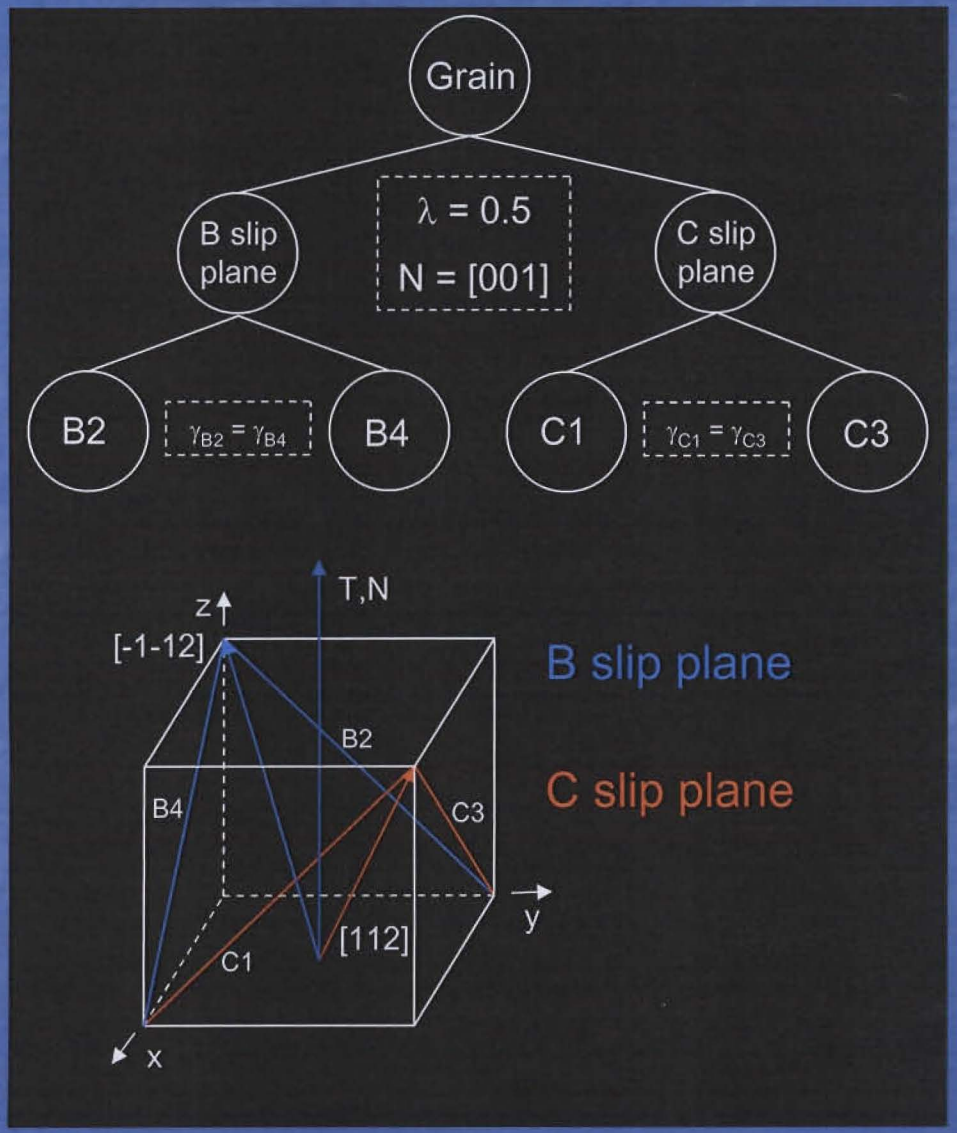


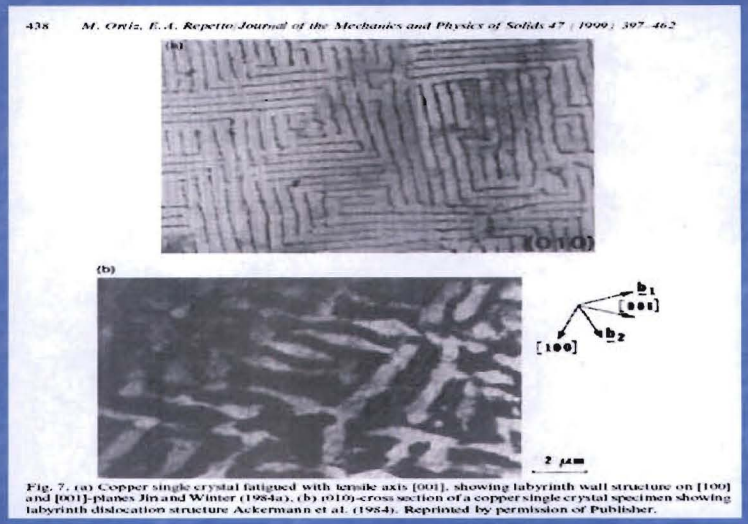


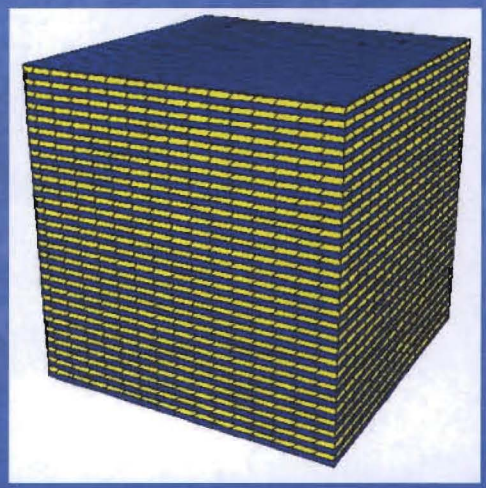

BL Hansen, 2008

# Size Dependency

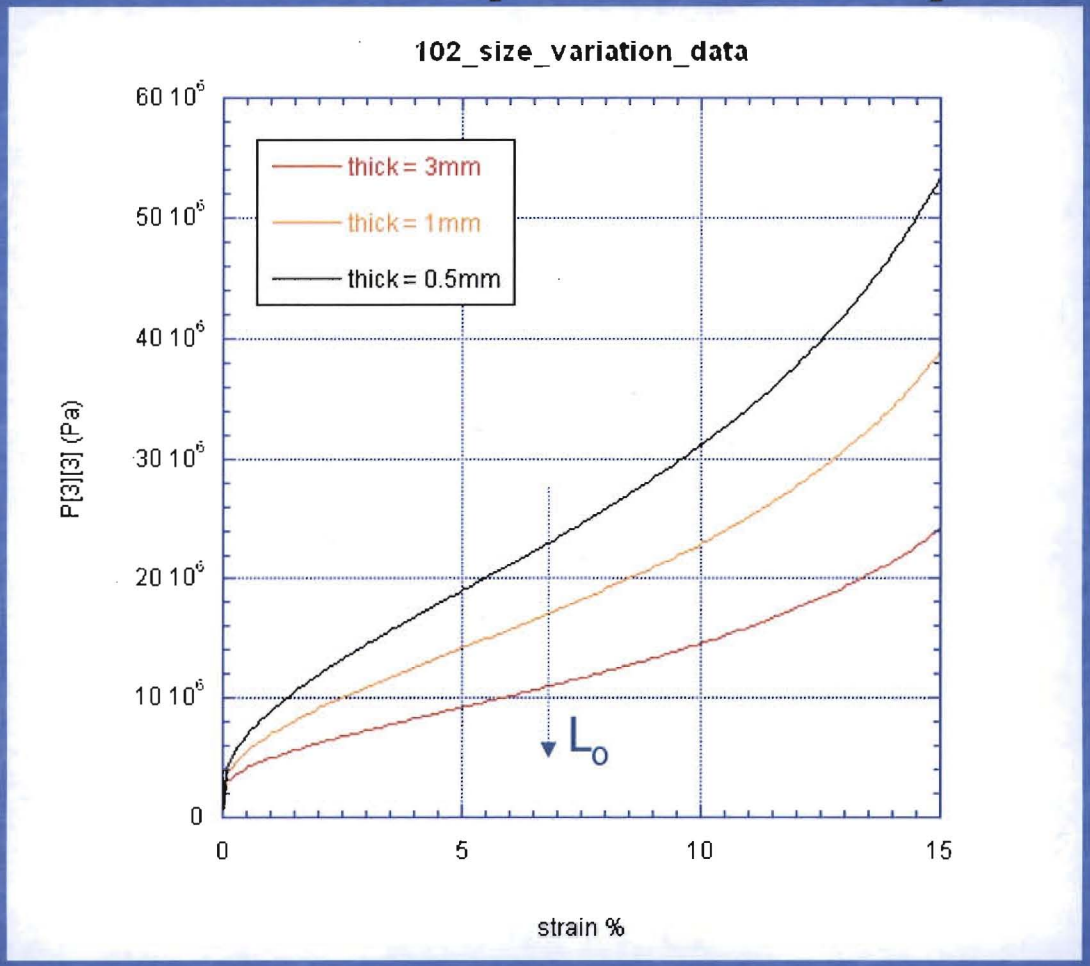


Variation in L for the 102 orientation simulations
-also gives shape dependency with shape to slip plane function

# Grain Shape

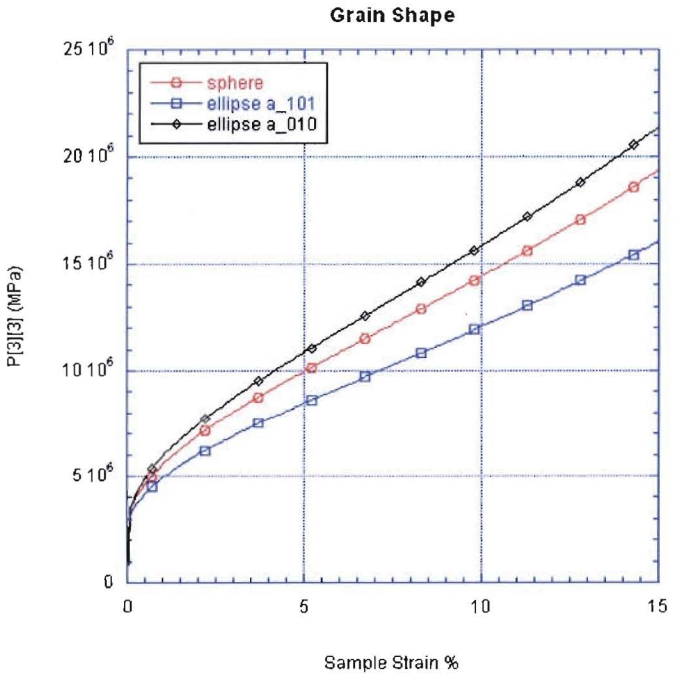


Grain shape with arrows indicating tensile ([101] crystal) direction:

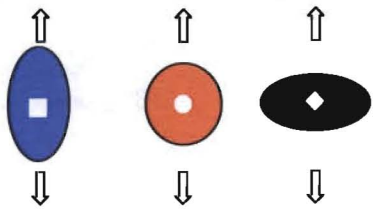

Not to scale

Grain shape influences the boundary layer and slip plane area, thus $\tau^c$

- Simulations with [101] crystal direction as tensile axis
- One simulation with a sphere, two simulation with an equal volume ellipsoid with major axis twice minor axis
  - Gives 5% more boundary layer
  - Either increases or decreases activated slip system dislocation mean free path lengths depending on ellipse orientation
  - Orientation of ellipsoid effects response

# Conclusions

- Behavior of symmetric microstructures are captured well.
- Correct predicted slip of evolving microstructures is captured. Hardening predicted by time evolution of subgrain structure length scale.
- Grain size and shape effect hardening behavior.
- Further work will likely need to include the time evolution of laminate volume fractions.

# 112 Structure